

1           **Cryo-EM structures of adenosine receptor A<sub>3</sub>AR bound to selective agonists**

2           Hongmin Cai<sup>1,7,\*</sup>, Shimeng Guo<sup>1,7</sup>, Youwei Xu<sup>1,7</sup>, Zhikan Xia<sup>1,7</sup>, Junrui Li<sup>1</sup>, Jun Sun<sup>1,2</sup>, Yi Jiang<sup>3</sup>,  
3           Xin Xie<sup>1,2,4,5,6,\*</sup>, H. Eric Xu<sup>1,2,5,\*</sup>

5           <sup>1</sup> State Key Laboratory of Drug Research, Shanghai Institute of Materia Medica, Chinese  
6           Academy of Sciences, Shanghai, China.

7           <sup>2</sup> University of Chinese Academy of Sciences, Beijing, China.

8           <sup>3</sup> Lingang Laboratory, Shanghai, China.

9           <sup>4</sup> School of Pharmaceutical Science and Technology, Hangzhou Institute for Advanced  
10          Study, University of Chinese Academy of Sciences, Hangzhou, China.

11          <sup>5</sup> School of Life Science and Technology, ShanghaiTech University, Shanghai, China.

12          <sup>6</sup> Shandong Laboratory of Yantai Drug Discovery, Bohai Rim Advanced Research Institute  
13          for Drug Discovery, Yantai, China

14          <sup>7</sup> These authors contributed equally: Hongmin Cai, Shimeng Guo, Youwei Xu, Zhikan Xia

16          \*Correspondence: [caihongmin@simm.ac.cn](mailto:caihongmin@simm.ac.cn) (H.C.); [xxie@simm.ac.cn](mailto:xxie@simm.ac.cn) (X.X.);  
17          [eric.xu@simm.ac.cn](mailto:eric.xu@simm.ac.cn) (H.E.X.)

19

**Abstract**

The adenosine A3 receptor (A<sub>3</sub>AR) belongs to a subfamily of G protein-coupled receptors and is an important therapeutic target for conditions including inflammation and cancer. The clinical compounds CF101 and CF102 are potent and selective A<sub>3</sub>AR agonists, but the structural basis of their recognition was unknown. Here we present the cryogenic electron microscopy structures of the full-length human A<sub>3</sub>AR bound to CF101 and CF102 at 3.3-3.2 Å resolution in complex with heterotrimeric G<sub>i</sub> protein. These agonists bind within the orthosteric pocket, with their adenine components engaging in conserved interactions while their substituted 3-iodobenzyl groups exhibit different orientations. Swapping extracellular loop 3 (ECL3) of A<sub>3</sub>AR onto other adenosine receptor subtypes enabled CF101/CF102 binding and receptor activation, and mutations in key residues, including His<sup>3.37</sup>, Ser<sup>5.42</sup> and Ser<sup>6.52</sup> that form a unique subpocket in A<sub>3</sub>AR, abolished receptor activation, highlighting these structural elements are critical for ligand selectivity. Compared to inactive A<sub>2A</sub>AR, the A<sub>3</sub>AR structures reveal conserved mechanism of receptor activation, including an outward shift of TM6. These structures provide key insights into molecular recognition and signaling mechanisms of A<sub>3</sub>AR, which should aid rational design of subtype-selective ligands targeting this important class of adenosine receptors.

20

21

22

23

24

25

26

27

28

29

30

31

32

33

34

35

36

37

## Introduction

The adenosine receptor subfamily of G protein-coupled receptors consists of four subtypes: A<sub>1</sub>, A<sub>2A</sub>, A<sub>2B</sub>, and A<sub>3</sub><sup>[1, 2]</sup>. These receptors are activated by the endogenous ligand, adenosine, to transduce downstream signals that mediate a number of important physiological and pathological roles including immunomodulation, energy balance, cardiac function, neuroprotection, etc<sup>[3-5]</sup>. A<sub>3</sub>AR is expressed in various tissues including the brain, heart, lungs, liver, kidneys, and immune cells<sup>[6]</sup>. Through its signaling functions, A<sub>3</sub>AR participates in regulating cardiac function, vasodilation, inhibition of inflammation, protection against ischemia-reperfusion injury, and suppression of oxidative stress. Additionally, A<sub>3</sub>AR is highly expressed in a number of tumor cells, suggesting its potential as a therapeutic target for suppressing cancer cell proliferation<sup>[6-8]</sup>.

48

The activation of A<sub>2A</sub>AR and A<sub>2B</sub>AR predominantly elicits stimulatory G protein (G<sub>s</sub>) signaling, while A<sub>1</sub>AR and A<sub>3</sub>AR exhibit a preference for coupling to inhibitory G protein (G<sub>i</sub>), leading to inhibition of adenylate cyclase and decreased intracellular cyclic AMP<sup>[2]</sup>. Based on the chemical structure of adenosine, numerous agonists and antagonists have been designed and tested against A<sub>3</sub>AR for disease indications such as cancer, inflammation, and pain<sup>[9]</sup> . Previous studies suggest that modifications at the N<sup>6</sup> position on the purine and 5'-N position on ribose group based on the adenosine framework yield potent A<sub>3</sub>AR agonists with high subtype selectivity<sup>[10-12]</sup>. CF101 and CF102 are representatives of such modification strategy with similar nucleoside core structure and only one chloro-substituent difference, both demonstrate high affinity and selectivity for A<sub>3</sub>AR<sup>[13-15]</sup>. CF101 showed efficacy in Phase III trials for psoriasis and rheumatoid arthritis<sup>[6]</sup> while CF102 is in clinical trials for hepatocellular carcinoma and non-alcoholic steatohepatitis (NASH)<sup>[16, 17]</sup>.

61

Adenosine receptors mediate many important functions and their wide expression makes subtype selectivity of ligands more critical to reduce possible side effects<sup>[18, 19]</sup>. Elucidating the structural basis of selective ligand binding to A<sub>3</sub>AR could help in improving the drug design process. To date, no A<sub>3</sub>AR structure has been reported. In this paper, we present the cryo-EM structures of A<sub>3</sub>AR bound to G<sub>i</sub> in the presence of CF101 and CF102, which reveals the basis of ligand recognition and ligand-induced activation mechanism of A<sub>3</sub>AR. Our works provide important insights for designing effective A<sub>3</sub>AR-targeted therapies, and more broadly for the subfamily of adenosine receptors.

70

71

## Results and Discussion

72

### Overall structures of the complexes

73

CF101 and CF102 are A<sub>3</sub>AR agonists containing modifications to the ribose and adenine moieties that confer potent binding to A<sub>3</sub>AR (Fig. 1a). Specifically, CF101 and CF102 have a

74

75 5'-N-methylcarboxamide substitution on the ribose group and a N<sup>6</sup>-(3-iodobenzyl) substitution  
76 on the adenine base (**Fig. 1a**). These modifications result in significantly higher A<sub>3</sub>AR potency  
77 compared to the endogenous A<sub>3</sub>AR agonist adenosine. We verified the selectivity of these  
78 nucleoside-derived compounds for A<sub>3</sub>AR versus other adenosine receptor subtypes  
79 (A<sub>1</sub>/A<sub>2A</sub>/A<sub>2B</sub>-AR) using NanoBiT association assays (**Fig. 1b-d**). While adenosine activated four  
80 subtypes with similar micromolar potencies, CF101 and CF102 displayed strongest potency  
81 of ~3 nM on A<sub>3</sub>AR but had weak or negligible response on other subtypes of adenosine  
82 receptors.

83  
84 We used NanoBiT tether strategy to stabilize the full-length A<sub>3</sub>AR-G protein complexes, as it  
85 has been used for many GPCR structural studies<sup>[20-22]</sup> (**Supplementary Fig. 1**). A<sub>3</sub>AR used in  
86 this study had an N-terminal thermostabilized apocytochrome b562RIL (BRIL) fusion to  
87 enhance its expression, which is co-expressed with G protein subunits and scFv16, an  
88 antibody fragment that is used to further stabilize the receptor G protein complex. For the  
89 CF101-A<sub>3</sub>AR-G<sub>i</sub> complex, data from 20,779 movies comprising 271,323 particles was used to  
90 determined the structure at 3.29 Å resolution (**Supplementary Fig. 2, Supplementary Table 1**).  
91 For the CF102-A<sub>3</sub>AR-G<sub>i</sub> complex, data from 13,581 movies yielding 283,561 particles was  
92 used to determined the structure at a resolution of 3.19 Å (**Supplementary Fig. 3,**  
93 **Supplementary Table 1**). The structures of the CF101/CF102-A<sub>3</sub>AR-G<sub>i</sub> complexes revealed  
94 that the ligands occupy the orthosteric binding pocket, with the core structures modeled clearly  
95 into the cryo-EM density at the center of the receptor transmembrane helicals (TMs) (**Fig. 1e-h**).  
96

97  
98 The structures showed the canonical seven-transmembrane architecture for A<sub>3</sub>AR, with the  
99 intracellular domains occupied by the α5 helix of Gα<sub>i</sub> for G<sub>i</sub> coupling. The density maps enabled  
100 modelling of most of the structures, except for A<sub>3</sub>AR N-terminus residues M1-L8, third  
101 intracellular loop N211-Y222, C-terminus V301-E318, and the alpha-helical domain of Gα<sub>i</sub>. The  
102 extracellular loop M151-S165 was also less defined but the backbone could be established  
103 (**Supplementary Fig. 4**). Aside from these regions, the models were well-resolved. Overall, the  
104 two agonist-bound complexes were highly similar, with 0.593 Å root mean square deviation  
105 (RMSD) for the whole receptor.

#### 106 107 **Binding mode of CF101/CF102 in A<sub>3</sub>AR orthosteric site**

108 The A<sub>3</sub>AR agonists CF101 and CF102 bind at conserved orthosteric pocket formed by ECL2,  
109 TM3, TM5, TM6 and TM7, akin to the endogenous ligand adenosine bound to other adenosine  
110 receptor subtypes (**Fig. 2a-b**). However, the orientations of the modified 3-iodobenzyl moieties  
111 differ between CF101 and CF102. The adenine core mediates conserved receptor interactions  
112 commonly seen in other adenosine receptors<sup>[21, 23, 24]</sup>. Notably, the adenine pyrimidine forms

113 π-stacks against F<sup>45.52</sup>, and the F<sup>45.52</sup>A mutation greatly affected the ability of CF101/CF102 to  
114 induce the receptor activation (Fig. 2c-f, Supplementary Table 2). Additionally, ribose and 3-  
115 iodophenyl groups form hydrogen bonds with polar side chains at positions 3.36, 6.55 and  
116 7.43, which are key for recognition of nucleoside ligands by all adenosine receptors (Fig. 2c-f,  
117 Supplementary Table 2).

118  
119 The ligand binding pocket is mainly composed of hydrophobic residues, including position  
120 3.33, 5.38, 5.47, 6.48, 6.51 and 7.39, which form hydrophobic contacts that are important for  
121 CF101/CF102 potencies (Fig. 2c-f, Supplementary Table 2). Alanine mutations at these  
122 positions severely reduced agonists' ability to induce receptor activation. His<sup>3.37</sup> and Ser<sup>5.42</sup>  
123 participate van der Waals contacts with the bound ligands, their alanine mutations also  
124 affected activity (Fig. 2c-f, Supplementary Table 2). The side chains from M174<sup>5.35</sup> and L264<sup>7.35</sup>  
125 in the receptor form hydrophobic interactions with the 3-iodophenyl group extended from the  
126 N<sup>6</sup> position of the adenosine base of CF101. In contrast, the corresponding group of CF102 is  
127 surrounded by V169<sup>ECL2</sup> and L264<sup>7.35</sup> from the receptor. Alanine mutations on these residues  
128 did not significantly affect the potency of the compounds on A<sub>3</sub>AR (Supplementary Fig. 6a,  
129 Supplementary Table 2), suggesting that the 3-iodophenyl substituents may exist alternative  
130 states at the receptor extracellular domains. This demonstrates that the N<sup>6</sup> position may  
131 accommodate various substituted groups through distinct conformations in the A<sub>3</sub>AR pocket.  
132

133 Moreover, CF102 is a 2-chloro derivative of CF101 (Fig. 1a). Y15<sup>1.35</sup> in CF102-bound A<sub>3</sub>AR  
134 forms hydrophobic contact with the 2-chloro group in CF102. Meanwhile, Y15<sup>1.35</sup> in A<sub>3</sub>AR  
135 formed π-π interaction with Y265<sup>7.36</sup> in TM7. The Y15<sup>1.35</sup>A mutation in A<sub>3</sub>AR abolishes the  
136 agonist activity of both CF102 and CF101 (Fig. 2c-f, Supplementary Table 2). According to the  
137 reports, modifications to the 2-position of the adenosine structure tend to well-tolerated in  
138 binding A<sub>3</sub>AR<sup>[14]</sup>, whether it a small or large group, even the macrocycle group linked with the  
139 group from N<sup>6</sup> moiety<sup>[25]</sup>. Elucidation of the subtle structural variations in ligand and receptor  
140 interactions thus provides molecular insight into the conformational adaptability and binding  
141 pose governing molecular recognition at A<sub>3</sub>AR.

#### 142 143 ECL3 in adenosine receptors

144 CF101 and CF102 show high selectivity on A<sub>3</sub>AR rather than other subtypes. Analysis the  
145 sequence of adenosine receptors reveals strong conservation within TMs, while the  
146 extracellular loops diverge among subtypes (Supplementary Fig. 5). ECL1 shows relatively  
147 distant from the orthosteric site. F168<sup>45.52</sup> in ECL2 provides the key π-π interactions with each  
148 agonists in adenosine receptors. However, A<sub>3</sub>AR possesses a shorter ECL3 than other  
149 subtypes (Fig. 3a). The shorter ECL3 may rigidify A<sub>3</sub>AR to minimize its conformational changes  
150 for specific ligand binding.

To assess the role of ECL3 in A<sub>3</sub>AR, we engineered chimeric receptors by grafting ECL3 from A<sub>3</sub>AR onto the backbones of other adenosine receptors. The chimeric receptors gained the ability to bind CF101 and CF102 with increased efficacy or potency (Fig. 3b-c, Supplementary Table 3). These findings suggest that ECL3 could serve as a structural factor mediating the selective recognition CF101 and CF102 by A<sub>3</sub>AR. According to the reported structure-activity relationship of ligands at the A<sub>3</sub>AR, numerous N<sup>6</sup>-substituted adenosine derivatives were synthesized. Too small or bulky groups at the N<sup>6</sup> position would reduce its potency or affinity on A<sub>3</sub>AR<sup>[13, 14]</sup>. The N<sup>6</sup> position on adenosine is projecting outwards into the binding pocket of A<sub>3</sub>AR and is in close spatial proximity to the ECL3 region of the A<sub>3</sub>AR. So the ECL3 loop is an important consideration in structure-activity studies of N<sup>6</sup>-modified adenosine derivatives against adenosine receptors. Delineating these subtle structural variations provides molecular insight into the selectivity of structurally analogous ligands for adenosine receptors.

#### **Binding pocket residues across adenosine receptors**

Furthermore, A<sub>3</sub>AR shared lowest identity with other subtypes among adenosine receptors. The sequence analysis reveals that the A<sub>3</sub>AR may confer selectivity through different residue types in the orthosteric binding pocket (Fig. 4a), which include residues at positions 3.32 (L/V/V/V, the residue in A<sub>3</sub>/A<sub>1</sub>/A<sub>2A</sub>/A<sub>2B</sub>-AR), 3.37 (H/Q/Q/Q), 5.42 (S/N/N/N), 5.47 (I/V/V/V), 6.52 (S/H/H/H) and 6.58 (I/T/T/T) (Fig. 4b, Supplementary Fig. 7). These residues in A<sub>3</sub>AR were mutated to the corresponding residues of other receptor subtypes, with aim to assess the impact of these A<sub>3</sub>AR mutants on the activity of CF101 and CF102 (Fig. 4c-d).

The leucine at position 3.32 in A<sub>3</sub>AR, versus valine in other subtypes, did not affect CF101/CF102 activity when mutated to valine, consistent with similar hydrophobic properties (Fig. 4c-d, Supplementary Fig. 7, Supplementary Table 2). Likewise, mutating isoleucine at positions 5.47 and 6.58 in A<sub>3</sub>AR to the valine and threonine found in other subtypes slightly impacted activation (Fig. 4c-d, Supplementary Table 2). This suggests that the slightly shorter side chains present in valine and threonine do not impair binding.

The side chain of H<sup>3.37</sup> and S<sup>5.42</sup> in A<sub>3</sub>AR form a hydrogen bond , which could not be formed by corresponding residues Q<sup>3.37</sup> and N<sup>5.42</sup> in other adenosine receptor subtypes (Fig. 4e-i). The H<sup>3.37</sup>Q mutation showed a limited impact on the activity of CF101/CF102 but the S<sup>5.42</sup>N mutation almost abolished the ability of CF101/CF102 to induce the receptor activation (Fig. 4c-d, Supplementary Table 2). Additionally, mutating S<sup>6.52</sup> to histidine (H) also severely decreased CF101 and CF102 activity, likely due to unfavorable steric or electronic properties of the longer histidine side chain (Fig. 4c-d, Supplementary Fig. 7, Supplementary Table 2). In contrast to other adenosine receptor subtypes, H<sup>3.37</sup>, S<sup>5.42</sup> and S<sup>6.52</sup> form a distinctive

189 subpocket in A<sub>3</sub>AR to accommodate the 5'-N-methylcarboxamide from the ribose (Fig. 4e-i,  
190 Supplementary Fig. 8). These results implicate this microdomain serves as a structural  
191 determinant for stabilizing CF101 and CF102 in A<sub>3</sub>AR versus other subtypes. Together, these  
192 findings demonstrate that minor sequence changes in the receptors could impact their  
193 conformations, thereby affecting ligand binding specificity.

194

### 195 **The activation mechanism of adenosine receptor A<sub>3</sub>AR**

196 Structural comparisons between active, agonist-bound A<sub>3</sub>AR complexes and an inactive,  
197 antagonist-bound A<sub>2A</sub>AR structure (PDB ID: 4EIY)<sup>[26]</sup> reveal hallmarks of conformational  
198 changes associated with GPCR activation<sup>[27, 28]</sup>. The A<sub>3</sub>AR structures exhibit an outward  
199 movement of TM6 compared to inactive A<sub>2A</sub>AR, shifting 11.6 Å based on measurements of  
200 residue Glu<sup>6.30</sup> at Cα atoms in receptors, analogous to movements seen in other activated  
201 class A GPCRs upon G protein coupling (Fig. 5a). Additional rearrangements of activation  
202 include inward movements of TM1 and TM7 and an upward shift of TM3 in A<sub>3</sub>AR relative to  
203 inactive A<sub>2A</sub>AR (Fig. 5b-d). The A<sub>3</sub>AR agonists CF101 and CF102 dock deeper into the  
204 orthosteric pocket compared to the A<sub>2A</sub>AR antagonist ZM-241385, enabling engagement of  
205 conserved GPCR activation motifs like the “toggle switch” on W<sup>6.48</sup> and transmission switch  
206 motifs D<sup>3.49</sup>R<sup>3.50</sup>Y<sup>3.51</sup> and N<sup>7.49</sup>P<sup>7.50</sup>xxY<sup>7.53</sup> (Fig. 5e-h). These microswitches trigger the  
207 conformational changes from the ligand binding pocket to the cytoplasmic G protein coupling  
208 interface. The series of structural transitions led to the rearrangements of receptor to enable  
209 G protein coupling and activation. By providing near-atomic resolution of A<sub>3</sub>AR activation  
210 mechanisms, these findings reveal fundamental insights into the relationship between ligand  
211 recognition in receptor, and activation of downstream signaling.

212

### 213 **G protein coupling of adenosine receptors**

214 All adenosine receptors exhibit differential G protein coupling preferences that correlate with  
215 distinct conformational orientations of the associated G proteins<sup>[21, 23, 24]</sup>. A<sub>1</sub>AR and A<sub>3</sub>AR  
216 preferentially couple to inhibitory G<sub>i</sub> proteins, while A<sub>2A</sub>AR and A<sub>2B</sub>AR primarily couple to  
217 stimulatory G<sub>s</sub> proteins to mediate intracellular signaling cascades (Fig. 6a). Structural  
218 comparisons reveal conformational differences between G<sub>i</sub>- and G<sub>s</sub>-coupled adenosine  
219 receptors complexes. Specifically, the TM6 helix of A<sub>1</sub>AR/A<sub>3</sub>AR-G<sub>i</sub> complexes shows a 3.1 Å  
220 inward shift to accommodate G<sub>i</sub> binding compared to A<sub>2A</sub>AR/A<sub>2B</sub>AR-G<sub>s</sub> complexes (Fig. 6b).  
221 Additionally, the α5 helix of Gα<sub>s</sub> subunits displays a 8.6 Å displacement relative to its  
222 orientation in G<sub>i</sub> complexes based on measurements of the Cα atom of Gα<sup>H5.03</sup> (Fig. 6c). The  
223 αN helix of Gα<sub>i</sub> exhibits a 3.3 Å tilt compared to G<sub>s</sub> when measuring the Cα of Gα<sup>HN.38</sup> (Fig. 6d).  
224 Overall, the structural arrangements of A<sub>1</sub>AR/A<sub>3</sub>AR-G<sub>i</sub> complexes closely resemble each other,  
225 similar to the consistency observed between A<sub>2A</sub>AR/A<sub>2B</sub>AR-G<sub>s</sub> complexes. These findings  
226 reveal that G<sub>i</sub>-coupled adenosine receptors adopt conserved G protein-binding conformations

227 that differ distinctly from those of G<sub>s</sub>-coupled adenosine receptors. Elucidation of the structural  
228 differences governing adenosine receptors-G protein interactions provides fundamental  
229 insights into the molecular determinants of G protein coupling specificity.  
230

231 **Conclusion**

232 In conclusion, we have determined the cryo-EM structures of the A<sub>3</sub>AR bound to selective  
233 agonists CF101 and CF102 with heterotrimeric G<sub>i</sub> protein. Despite the conserved binding of  
234 the core adenosine moiety, the structures revealed differences in the orientations of the N<sup>6</sup>  
235 substituted groups in CF101 and CF102. We identified ECL3 and key pocket residues His<sup>3,37</sup>,  
236 Ser<sup>5,42</sup> and Ser<sup>6,52</sup> that confer selectivity over other adenosine receptor subtypes by  
237 mutagenesis studies. Comparison to an inactive A<sub>2A</sub>AR structure provided insight into the  
238 conformational changes associated with A<sub>3</sub>AR activation and G protein coupling. By  
239 elucidating the molecular mechanisms governing ligand recognition, signaling, and subtype  
240 selectivity, A<sub>3</sub>AR structures significantly advance our fundamental understanding of this  
241 important drug target. The findings pave the way for structure-guided design of improved  
242 therapeutics targeting adenosine receptors for the treatment of cancer, inflammation, and  
243 other diseases.

244  
245 **Acknowledgements**

246 We thanks Wen Hu, Kai Wu and Qingning Yuan from the Shanghai Advanced Center for  
247 Elecron Microscopy (Shanghai Institute of Materia Medica, Chinese Academy of Sciences) for  
248 their technical supporting and assistance with cryo-EM dataset collection. This project was  
249 supported by the CAS Strategic Priority Research Program (XDB37030103 to H.E.X.);  
250 Shanghai Municipal Science and Technology Major Project (H.E.X.); The National Natural  
251 Science Foundation of China (82121005 to X.X., Y.J., and H.E.X., 32130022 to H.E.X.,  
252 82330113 to X.X., 32301004 to H.C., 82304579 to S.G., and 32171187 to Y.J.); Shanghai  
253 Municipal Science and Technology Major Project (2019SHZDZX02 to H.E.X.); the Lingang  
254 Laboratory (LG-GG-202204-01 to H.E.X.); the National Key R&D Program of China  
255 (2018YFA0507002 to H.E.X.); China Postdoctoral Science Foundation (2021M703341,  
256 2023T160662 to H.C.).

257  
258 **Author Contributions**

259 H. C. designed the expression constructs, purified the protein complexes supervised by  
260 H.E.X.. Y.X. and H.C. prepared the grids and performed the cryo-EM data processing and  
261 model building with the help of J.L.. H.E.X., Y.J. and H.C. analyzed the structures. S.G. and  
262 Z.X. performed the functional studies with the help of J.S. under the supervision of X.X.. H.C.  
263 prepared the figures and manuscript. Y.X. and S.G. contributed to manuscript preparation.  
264 H.E.X. and H.C. wrote the manuscript with input from all authors.

**265 Data availability**

266 The atomic coordinates of CF101/CF102-A3AR-Gi complex have been deposited in the  
267 Protein Data Bank (<http://www.rcsb.org>) with accession codes xxxx and xxxx, respectively.  
268 The corresponding cryo-EM density maps have been deposited in the Electron Microscopy  
269 Data Bank (<https://www.ebi.ac.uk/pdbe/emdb/>) with accession codes EMD-xxxxxx and EMD-  
270 xxxx, respectively.

**271 Competing interests**

272 The authors declare no competing interests.

273

274

275           **References**

- 276       1. Salvatore, CA, MA Jacobson, HE Taylor, J Linden and RG Johnson, Molecular cloning and  
277           characterization of the human A3 adenosine receptor. *Proc Natl Acad Sci U S A*, 1993. 90(21):  
278           10365-9.
- 279       2. Sheth, S, R Brito, D Mukherjea, LP Rybak and V Ramkumar, Adenosine receptors: expression,  
280           function and regulation. *Int J Mol Sci*, 2014. 15(2): 2024-52.
- 281       3. Borea, PA, K Varani, F Vincenzi, PG Baraldi, MA Tabrizi, S Merighi and S Gessi, The A3  
282           adenosine receptor: history and perspectives. *Pharmacol Rev*, 2015. 67(1): 74-102.
- 283       4. Jacobson, KA, S Merighi, K Varani, PA Borea, S Baraldi, M Aghazadeh Tabrizi, R Romagnoli,  
284           PG Baraldi, et al., A(3) Adenosine Receptors as Modulators of Inflammation: From Medicinal  
285           Chemistry to Therapy. *Med Res Rev*, 2018. 38(4): 1031-1072.
- 286       5. Hauser, AS, AJ Kooistra, C Munk, FM Heydenreich, DB Veprintsev, M Bouvier, MM Babu and  
287           DE Gloriam, GPCR activation mechanisms across classes and macro/microscales. *Nat Struct  
288           Mol Biol*, 2021. 28(11): 879-888.
- 289       6. Fishman, P, S Bar-Yehuda, BT Liang and KA Jacobson, Pharmacological and therapeutic  
290           effects of A3 adenosine receptor agonists. *Drug Discov Today*, 2012. 17(7-8): 359-66.
- 291       7. Fishman, P, S Bar-Yehuda, L Madi and I Cohn, A3 adenosine receptor as a target for cancer  
292           therapy. *Anticancer Drugs*, 2002. 13(5): 437-43.
- 293       8. Marwein, S, B Mishra, UC De and PC Acharya, Recent Progress of Adenosine Receptor  
294           Modulators in the Development of Anticancer Chemotherapeutic Agents. *Curr Pharm Des*,  
295           2019. 25(26): 2842-2858.
- 296       9. Fishman, P, Drugs Targeting the A3 Adenosine Receptor: Human Clinical Study Data. *Molecules*,  
297           2022. 27(12).
- 298       10. Jacobson, KA, Adenosine A3 receptors: novel ligands and paradoxical effects. *Trends  
299           Pharmacol Sci*, 1998. 19(5): 184-91.
- 300       11. Jacobson, KA, AM Klutz, DK Tosh, AA Ivanov, D Preti and PG Baraldi, Medicinal chemistry of  
301           the A3 adenosine receptor: agonists, antagonists, and receptor engineering. *Handb Exp  
302           Pharmacol*, 2009(193): 123-59.
- 303       12. Barkan, K, P Lagarias, M Stampelou, D Stamatis, S Hoare, D Safitri, KN Klotz, E Vrontaki, et  
304           al., Pharmacological characterisation of novel adenosine A(3) receptor antagonists. *Sci Rep*,  
305           2020. 10(1): 20781.
- 306       13. Gallo-Rodriguez, C, XD Ji, N Melman, BD Siegman, LH Sanders, J Orlina, B Fischer, Q Pu, et  
307           al., Structure-activity relationships of N6-benzyladenosine-5'-uronamides as A3-selective  
308           adenosine agonists. *J Med Chem*, 1994. 37(5): 636-46.
- 309       14. Kim, HO, XD Ji, SM Siddiqi, ME Olah, GL Stiles and KA Jacobson, 2-Substitution of N6-  
310           benzyladenosine-5'-uronamides enhances selectivity for A3 adenosine receptors. *J Med Chem*,  
311           1994. 37(21): 3614-21.
- 312       15. Van Schaick, EA, KA Jacobson, HO Kim, IJ AP and M Danhof, Hemodynamic effects and  
313           histamine release elicited by the selective adenosine A3 receptor agonist 2-Cl-IB-MECA in  
314           conscious rats. *Eur J Pharmacol*, 1996. 308(3): 311-4.
- 315       16. Suresh, RR, S Jain, Z Chen, DK Tosh, Y Ma, MC Podszun, Y Rotman, D Salvemini, et al.,  
316           Design and in vivo activity of A(3) adenosine receptor agonist prodrugs. *Purinergic Signal*, 2020.  
317           16(3): 367-377.

- 318 17. Fishman, P, S Cohen, I Itzhak, J Amer, A Salhab, F Barer and R Safadi, The A3 adenosine  
319 receptor agonist, namodenoson, ameliorates non-alcoholic steatohepatitis in mice. *Int J Mol*  
320 *Med*, 2019. 44(6): 2256-2264.
- 321 18. Jacobson, KA and ZG Gao, Adenosine receptors as therapeutic targets. *Nat Rev Drug Discov*,  
322 2006. 5(3): 247-64.
- 323 19. Verzijl, D and AP Ijzerman, Functional selectivity of adenosine receptor ligands. *Purinergic*  
324 *Signal*, 2011. 7(2): 171-92.
- 325 20. Duan, J, DD Shen, XE Zhou, P Bi, QF Liu, YX Tan, YW Zhuang, HB Zhang, et al., Cryo-EM  
326 structure of an activated VIP1 receptor-G protein complex revealed by a NanoBiT tethering  
327 strategy. *Nat Commun*, 2020. 11(1): 4121.
- 328 21. Cai, H, Y Xu, S Guo, X He, J Sun, X Li, C Li, W Yin, et al., Structures of adenosine receptor  
329 A(2B)R bound to endogenous and synthetic agonists. *Cell Discov*, 2022. 8(1): 140.
- 330 22. Duan, J, H Liu, F Zhao, Q Yuan, Y Ji, X Cai, X He, X Li, et al., GPCR activation and GRK2  
331 assembly by a biased intracellular agonist. *Nature*, 2023. 620(7974): 676-681.
- 332 23. Lebon, G, T Warne, PC Edwards, K Bennett, CJ Langmead, AG Leslie and CG Tate, Agonist-  
333 bound adenosine A2A receptor structures reveal common features of GPCR activation. *Nature*,  
334 2011. 474(7352): 521-5.
- 335 24. Draper-Joyce, CJ, R Bhola, J Wang, A Bhattacharai, ATN Nguyen, I Cowie-Kent, K O'Sullivan, LY  
336 Chia, et al., Positive allosteric mechanisms of adenosine A(1) receptor-mediated analgesia.  
337 *Nature*, 2021. 597(7877): 571-576.
- 338 25. Tosh, DK, CL Fisher, V Salmaso, TC Wan, RG Campbell, E Chen, ZG Gao, JA Auchampach,  
339 et al., First Potent Macroyclic A(3) Adenosine Receptor Agonists Reveal G-Protein and beta-  
340 Arrestin2 Signaling Preferences. *ACS Pharmacol Transl Sci*, 2023. 6(9): 1288-1305.
- 341 26. Jaakola, VP, MT Griffith, MA Hanson, V Cherezov, EY Chien, JR Lane, AP Ijzerman and RC  
342 Stevens, The 2.6 angstrom crystal structure of a human A2A adenosine receptor bound to an  
343 antagonist. *Science*, 2008. 322(5905): 1211-7.
- 344 27. Zhou, Q, D Yang, M Wu, Y Guo, W Guo, L Zhong, X Cai, A Dai, et al., Common activation  
345 mechanism of class A GPCRs. *Elife*, 2019. 8.
- 346 28. Mazziotta, C, JC Rotondo, C Lanzillotti, G Campione, F Martini and M Tognon, Cancer biology  
347 and molecular genetics of A(3) adenosine receptor. *Oncogene*, 2022. 41(3): 301-308.

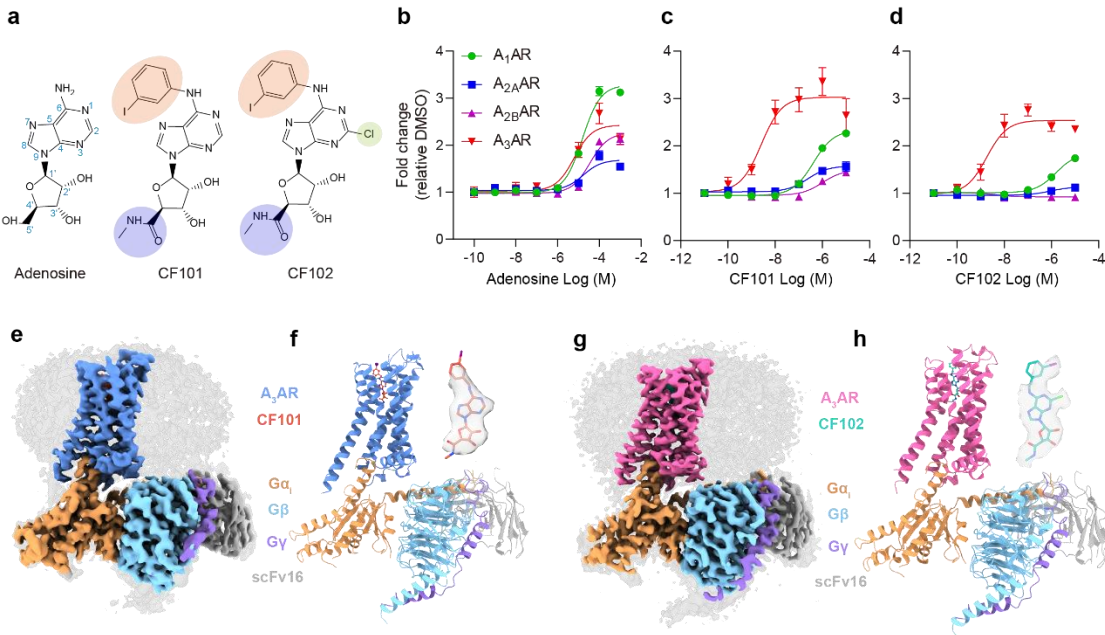


**Fig 1. Cryo-EM structures of CF101-A<sub>3</sub>AR-G<sub>i</sub> and CF102-A<sub>3</sub>AR-G<sub>i</sub> complexes.**

a. Chemical structures of the adenosine, CF101 and CF102. Highlighting modifications at the 5'-N-methylcarboxamide in the ribose group and N<sup>6</sup> and C2 positions of the adenosine group. The atom numbering was indicated in blue. CF101, is also named IB-MECA and N<sup>6</sup>-(3-iodobenzyl)adenosine-5'-N-methyluronamide. CF102, is also named CI-IB-MECA and 2-chloro-N<sup>6</sup>-(3-iodobenzyl)adenosine-5'-N-methyluronamide. b-d. NanoBiT association assays monitoring ligand activity on adenosine receptors for adenosine (b), CF101 (c) and CF102 (d) from three independent experiments in triplicate (n=3). e, f. Cryo-EM map (e) and model (f) of the CF101-A<sub>3</sub>AR-G<sub>i</sub> complex, with inset showing CF101 density. The density map in the inset is shown at 0.232 threshold. g, h. Cryo-EM map (g) and model (h) of the CF102-A<sub>3</sub>AR-G<sub>i</sub> complex, with inset showing CF102 density. The density map in the inset is shown at 0.17 threshold. Subunits are colored as indicated.

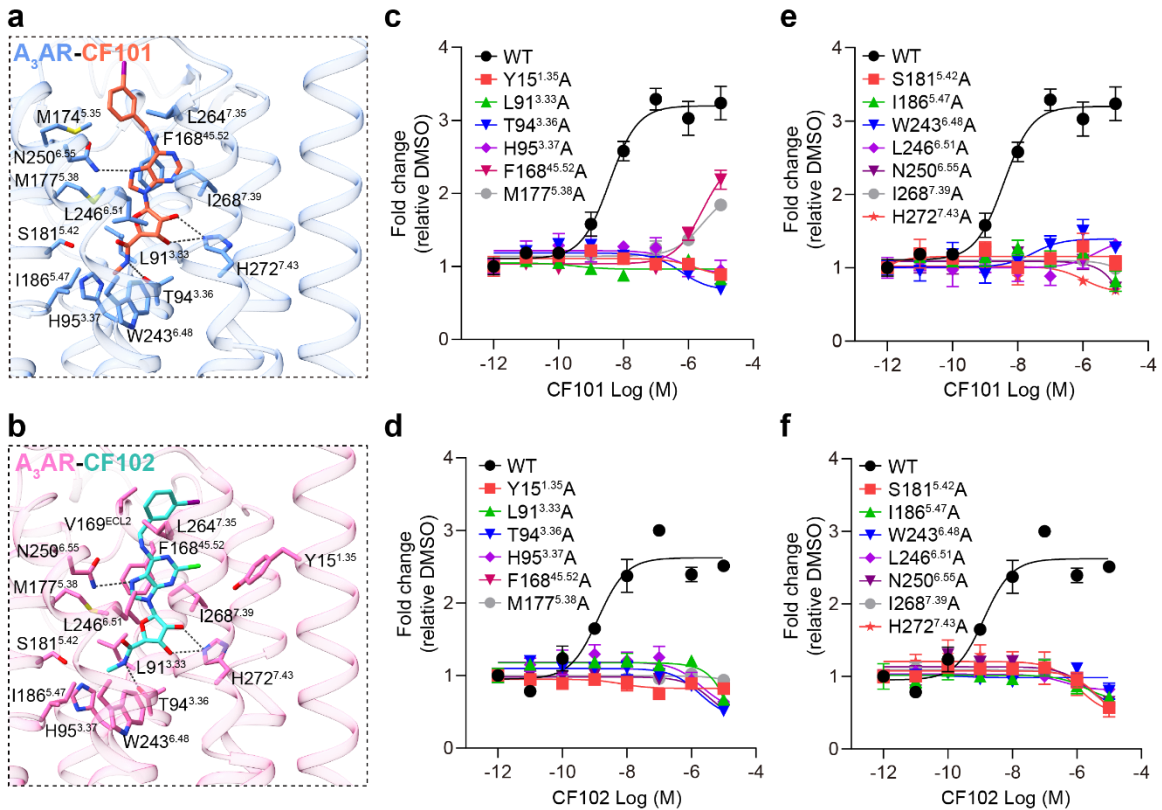


**Fig 2. The orthosteric binding pocket.**

**a, b** Detailed interactions between A<sub>3</sub>AR and CF101 (**a**) or CF102 (**b**) from the membrane plane. Residues involved in ligand interaction are colored blue and pink in two complexes, respectively. Black dashed lines indicate hydrogen bonds. **c-f** Dose-response curves of mutants of A<sub>3</sub>AR induced by CF101 (upper panels, **c, e**) or CF102 (lower panels, **d, f**) using NanoBiT assay.

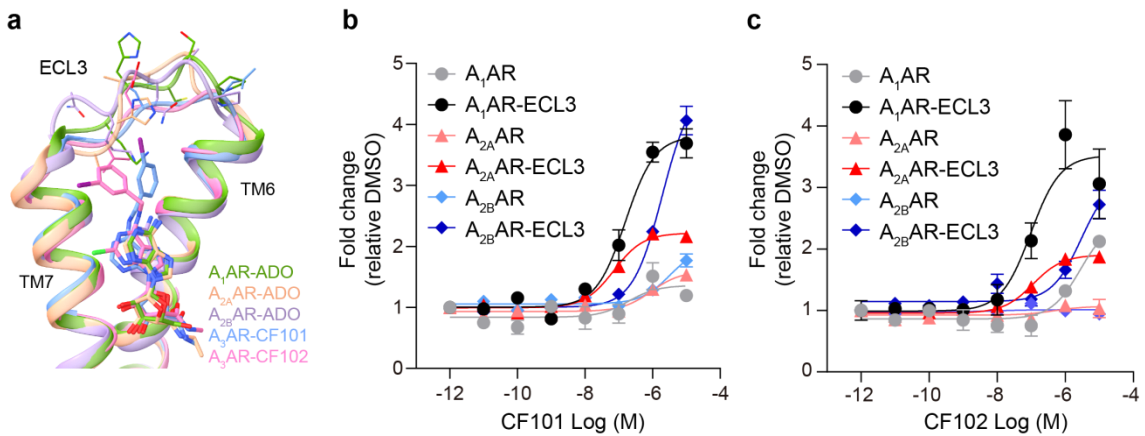


**Fig 3. Swapping ECL3 increases CF101/CF102 potency at adenosine A<sub>1</sub>/A<sub>2A</sub>/A<sub>2B</sub> receptor subtypes.**

**a** Superposition of ECL3 in the adenosine receptors shows A<sub>3</sub>AR reveals A<sub>3</sub>AR has a shorter ECL3. Other TMs were omitted. **b, c** Effects of CF101 and CF102 were tested on the A<sub>1</sub>AR, A<sub>2A</sub>AR, and A<sub>2B</sub>AR and their corresponding mutants containing the swapped ECL3 from the A<sub>3</sub>AR using NanoBiT assays.

373

374

375

376

377

378

379

380

381

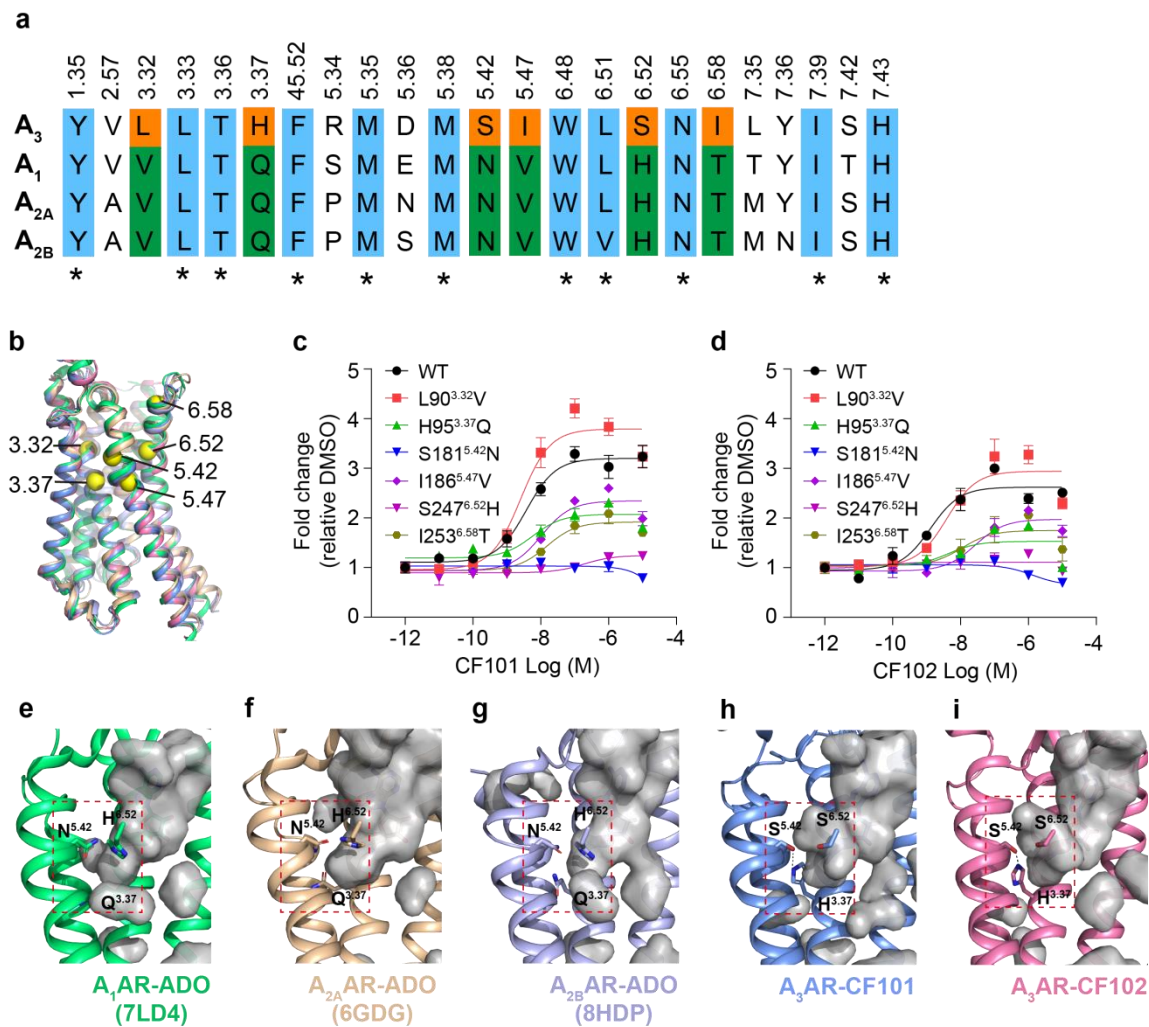


**Fig 4. Key residues in the A<sub>3</sub>AR binding pocket.**

382  
383  
384 **a** Sequence alignment of the residues in the orthosteric binding pocket among the adenosine  
385 receptors. The conserved residues were colored with blue and stars marked. The unique  
386 residues in A<sub>3</sub>AR, different from other adenosine receptors subtypes were colored in orange,  
387 while the others subtypes at corresponding position were colored in green. All residues were  
388 annotated based on GPCR Ballesteros-Weinstein numbering scheme. **b** Superposition of  
389 adenosine receptors, the unique residues in A<sub>3</sub>AR from the other adenosine receptors are  
390 shown as yellow ball. **c-d** Effects of CF101/CF102 on A<sub>3</sub>AR mutants containing swapped  
391 residues from other adenosine receptors by NanoBiT assay. **e-i** The binding cavities of the  
392 adenosine receptors are generated in PyMOL, the cavities were depicted as gray. In A<sub>3</sub>AR,  
393 His<sup>3.37</sup>, Ser<sup>5.42</sup> and Ser<sup>6.52</sup> form a subpocket, whereas these positions are conserved as  
394 Gln<sup>3.37</sup>, Asn<sup>5.42</sup> and His<sup>6.52</sup> in the other adenosine receptor subtypes, respectively (His, H;  
395 Ser, S; Gln, Q; Asn, N). Dash lines in **h** and **i** showed the hydrogen bonds between His<sup>3.37</sup>  
396 and Ser<sup>5.42</sup>.

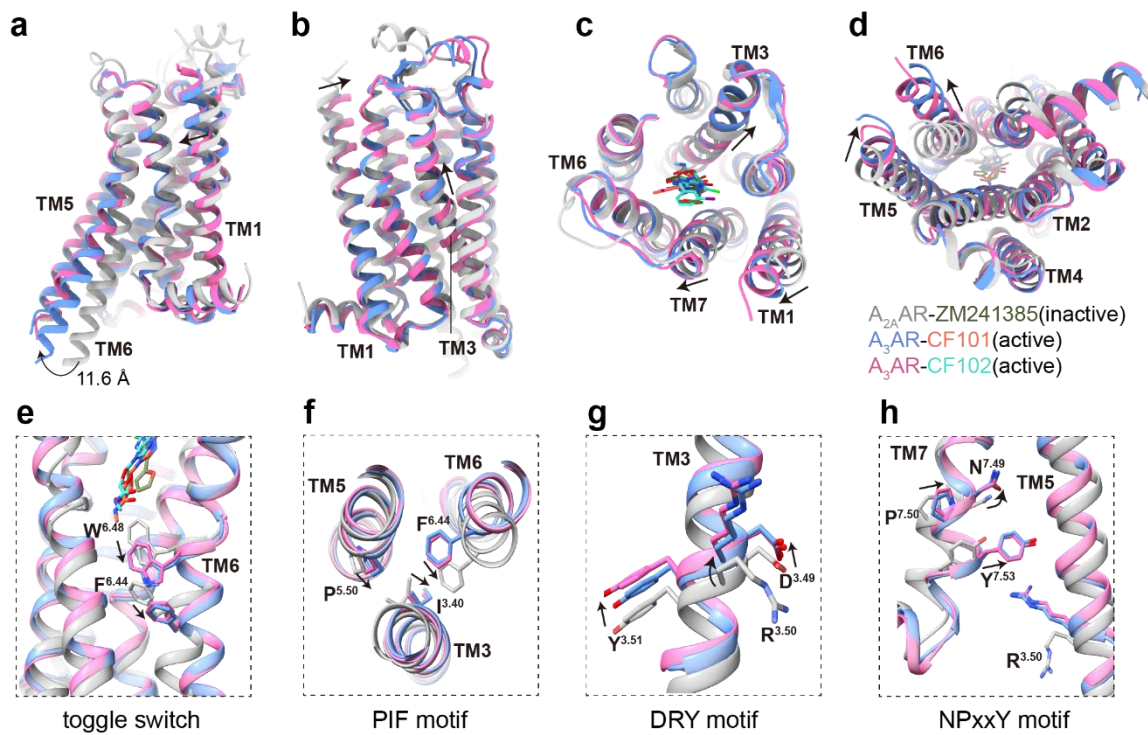


**Fig 5. A<sub>3</sub>AR activation mechanism.**

**a-b** Superposition of active A<sub>3</sub>AR-CF101/CF102 complexes (blue/pink) with inactive A<sub>2A</sub>AR-ZM241385 complex (grey, PDB ID 4EIY). **c,d** Comparison of extracellular (**c**) and cytoplasmic (**d**) views of active A<sub>3</sub>AR and inactive A<sub>2A</sub>AR. **e-g** Conformational changes in conserved motifs, including toggle switch, PIF, DRY and NPxxY, upon CF101/CF102 binding to A<sub>3</sub>AR relative to inactive A<sub>2A</sub>AR-ZM241385. Arrows indicate movement directions.

404  
405  
406  
407  
408  
409  
410  
411

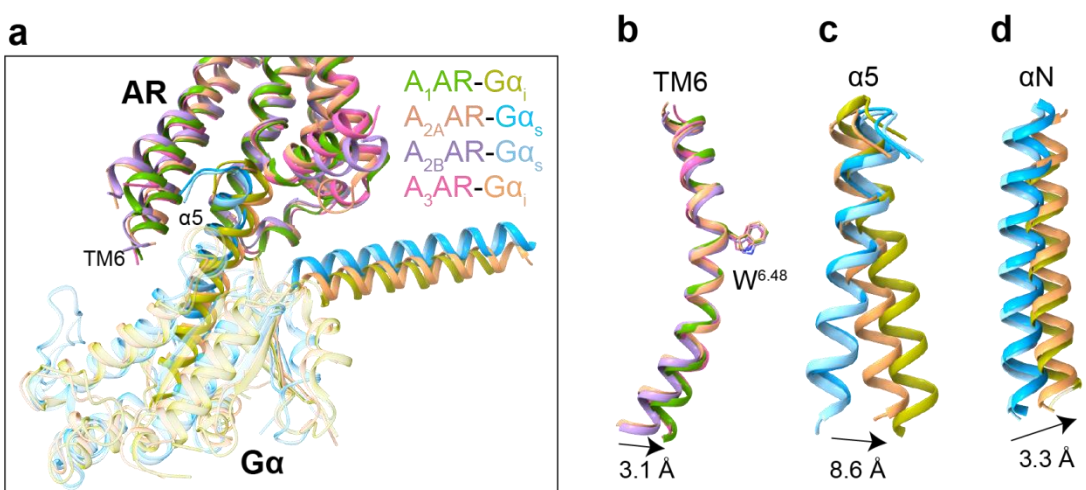


**Figure 6. G protein coupling of adenosine receptors.**

**a** Comparison of G protein conformations in A<sub>1</sub>/A<sub>3</sub>AR-G<sub>i</sub> and A<sub>2A</sub>/A<sub>2B</sub>AR-G<sub>s</sub> complexes. **b** Conformational comparison of TM6 in adenosine receptors, referencing toggle switch W<sup>6.48</sup> in TM6 of receptor. **c-d** Conformational comparison of α5 helix and αN helix in G protein adenosine receptors-G protein complexes. Arrows indicate movement directions.

412      **Methods**

413      **Construct design**

414      The full-length gene coding human A<sub>3</sub>AR was synthesized (Synbio) and subcloned into  
415      pFastBac vector using CloneExpress II one step cloning kit (Vazyme Biotech). A hemagglutinin  
416      signal peptide and thermostabilized apocytochrome b562RIL (BRIL) were fused at the N-  
417      terminal of A<sub>3</sub>AR to enhance receptor expression. To enhance complex stability, a NanoBiT  
418      tethering approach was used where an LgBiT domain was fused to the C-terminal of the  
419      receptor<sup>[20]</sup>. A dual maltose-binding protein was linked after LgBiT through a tobacco etch virus  
420      protease site (TEV site) for further cleavage. A dominant-negative mutant of bovine Gα<sub>i</sub>  
421      containing G203A/A326S<sup>[29]</sup> mutations was generated to stabilize the heterotrimeric Gα<sub>i</sub>βγ  
422      protein. Rat Gβ1 was fused with a HiBiT at C-terminal for structural complementation of LgBiT  
423      to form a NanoBiT. The single-chain variable fragment scFv16 was applied to bind the Gα<sub>i</sub>βγ  
424      protein for stabilization<sup>[30]</sup>. Gα<sub>i</sub>, Gβ1-HiBiT, Gγ, and scFv16, were cloned into pFastBac vector  
425      (**Supplementary Fig. 1a**), respectively.

426      **Protein expression and purification**

427      The recombinant A<sub>3</sub>AR, Gα<sub>i</sub>, Gβ1-HiBiT, Gγ, and scFv16 were co-expressed in *Trichoplusia ni*  
428      High Five insect cells using the Bac-to-Bac baculovirus expression system. High Five cells  
429      were co-infected with the baculovirus at a cell density of  $3.5 \times 10^6$  cells per milliliter. Forty-  
430      eight hours later, the infected cells were harvested and stored at -80 °C until used.

431      For the purification of the CF101-A<sub>3</sub>AR-G<sub>i</sub> complex, cells pellets were thawed and resuspended  
432      in Buffer A (100 mM NaCl, 20 mM HEPES, pH 7.5) supplemented with protease inhibitor  
433      cocktail (TargetMol). Cells were lysed by dounce homogenization followed by centrifugation to  
434      remove insoluble materials. The pellets were resuspended in Buffer B (100 mM NaCl, 10 % (v/v)  
435      glycerol, 20 mM HEPES, pH 7.5) supplemented with 10 mM MgCl<sub>2</sub>, 5 mM CaCl<sub>2</sub>, 0.2 mM Tris-  
436      (2-carboxyethyl)phosphine (TCEP, Hampton Research) and protease inhibitor cocktail. The  
437      complex was formed by rotating at room temperature for 1 h after addition of 25 mU/mL  
438      apyrase and 10 μM CF101. After incubation, the sample was solubilized in 0.5 % (w/v) lauryl  
439      maltose neopentylglycol (LMNG, Anatrace) and 0.1% (w/v) cholestryl hemisuccinate (CHS,  
440      Anatrace) for 3 h at 4 °C. The supernatant was clarified by centrifugation at 100,000× g for 40  
441      min. The supernatant was incubated with dextrin beads 6FF (Smart-Lifescience) for 3 h at 4 °C.  
442      The beads were loaded onto a gravity column and washed with 20 column volumes of Buffer  
443      C (100 mM NaCl, 2 mM MgCl<sub>2</sub>, 10 μM CF101, 0.2 mM TCEP, 0.01 % (w/v) LMNG, 0.002 % (w/v)  
444      CHS, 20 mM HEPES, pH 7.5). The complex was eluted with Buffer C supplemented with 10  
445      mM maltose and further concentrated using 100 kDa molecular weight cut-off concentrator.  
446      TEV protease was added to the concentrated protein at 4 °C overnight to cleave dual maltose  
447      binding protein from fusion protein. After digestion, sample was loaded onto Superdex 200  
448  
449

450 Increase 10/300 GL column (GE Healthcare) with Buffer D (100 mM NaCl, 2 mM MgCl<sub>2</sub>, 10  
451 µM CF101, 0.1 mM TCEP, 0.00075 %(w/v) LMNG, 0.00025 %(w/v) glyco-diosgenin,  
452 0.0002 %(w/v) CHS, 20 mM HEPES, pH 7.5). The desired fractions were pooled and  
453 concentrated to 5-8 mg/mL for cryo-EM sample preparation.

454

### 455 **Cryo-EM data collection**

456 Cryo-EM grids were prepared with the Vitrobot Mark IV plunger (FEI) set to 8 °C and 100%  
457 humidity. Three-microliters of the CF101-A<sub>3</sub>AR-G<sub>i</sub> complex were applied to glow- discharged  
458 Quantifoil R1.2/1.3 holey carbon grids. The sample was incubated for 10 s on the grids before  
459 blotting for 3.5 s (double-sided, blot force 1) and flash-frozen in liquid ethane immediately. The  
460 same conditions were used for the CF101-A<sub>3</sub>AR-G<sub>i</sub> complex sample.

461

462 For CF101-A<sub>3</sub>AR-G<sub>i</sub> complex, three datasets comprising 20,779 movies were collected on a  
463 Titan Krios equipped with a Gatan K3 direct electron detection device at 300 kV with a  
464 magnification of 105,000 corresponding to a pixel size 0.824 Å. Image acquisition was  
465 performed with EPU Software (FEI Eindhoven, Netherlands). We collected a total of 36 frames  
466 accumulating to a total dose of 50 e<sup>-</sup> Å<sup>-2</sup> over 2.5 s exposure.

467

468 For CF102-A<sub>3</sub>AR-G<sub>i</sub> complex dataset, two datasets totaling 13,581 movies were collected on  
469 a Titan Krios equipped with a Gatan K3 detector at 300 kV with a magnification of 105,000 and  
470 pixel size of 0.824 Å, using EPU Software (FEI Eindhoven, Netherlands). Thirty-six frames  
471 were collected over a 2.5-s exposure to a dose of 50 e<sup>-</sup> Å<sup>-2</sup>.

472

### 473 **Image processing**

474 MotionCor2 was used to perform the frame-based motion-correction algorithm to generate  
475 drift-corrected micrograph for further processing, and CTFFIND4 provided estimation of  
476 contrast transfer function (CTF) parameters<sup>[31, 32]</sup>.

477

478 For the CF101-A<sub>3</sub>AR-G<sub>i</sub> dataset, the previously resolved structure of BAY 60-6583-A<sub>2B</sub>AR-G<sub>s</sub>  
479<sup>[21]</sup> was used as a reference for automatic particle picking in Relion 3.0<sup>[33]</sup>. Particle picking and  
480 extraction yielded 4,550,294 particles after 2D classification clearance, which were imported  
481 into cryoSPARC<sup>[34]</sup>. Four rounds of 2D classification selected 1,267,837 particles, followed by  
482 two rounds of 3D heterogenous refinement giving 982,833 particles. After two additional  
483 rounds of 2D classification and two rounds of heterogenous refinement, 271,323 particles were  
484 refined to a structure at 3.29 Å global resolution using non-uniform refinement (**Supplementary**  
485 **Fig. 2**).

486

487 For CF102-A<sub>3</sub>AR-G<sub>i</sub> complex dataset, the BAY 60-6583-A<sub>2B</sub>AR-G<sub>s</sub> structure<sup>[21]</sup> was again used  
488 for reference-based particle picking. 4,090,959 and 4,833,382 particles were autopicked and  
489 extracted from Dataset1 and Dateset2, respectively. For Dataset1, two rounds of 2D  
490 classification were used to separate out 1,070,085 particles. Masked 3D classification on the  
491 receptor part was used to separate out 175,747 particles that resulted to a clearer density of  
492 A<sub>3</sub>AR. For Dataset2, two rounds of 2D classification and two rounds of 3D classification were  
493 performed to separate out 246,392 particles. After clearance, the remained particles from two  
494 datasets were combined and subjected to alignment-free 3D classification. 283,561 particles  
495 were remained and transferred in cryoSPARC<sup>[34]</sup>. One round of heterogenous refinement  
496 yielded a final 102,581 particle were refined to a structure at 3.19 Å global resolution using  
497 non-uniform refinement (**Supplementary Fig. 3**).  
498

#### 499 **Model building**

500 An A<sub>3</sub>AR structure predicted by AlphaFold2 was used as the starting reference models for  
501 receptors building<sup>[35]</sup>. Structures of Gα<sub>i</sub>, Gβ, Gγ and the scFv16 were derived from PDB entry  
502 7EZH<sup>[36]</sup> were rigid body fit into the density. All models were fitted into the EM density map  
503 using UCSF Chimera<sup>[37]</sup> followed by iterative rounds of manual adjustment and automated  
504 rebuilding in COOT<sup>[38]</sup> and PHENIX<sup>[39]</sup>, respectively. The model was finalized by rebuilding in  
505 ISOLDE<sup>[40]</sup> followed by refinement in PHENIX with torsion-angle restraints to the input model.  
506 The final model statistics were validated using Comprehensive validation (cryo-EM) in PHENIX  
507 and provided in the supplementary information, **Supplementary Table 1**. All structural figures  
508 were prepared using Chimera<sup>[37]</sup>, Chimera X<sup>[41]</sup>, and PyMOL (Schrödinger, LLC.).  
509  
510

#### 511 **NanoBiT assay**

512 To monitor G protein interaction with A<sub>1</sub>AR, A<sub>2A</sub>AR, A<sub>2B</sub>AR or A<sub>3</sub>AR upon agonist stimulation,  
513 a NanoLuc-based NanoBiT enzyme complementation assay was used (Promega). The C-  
514 terminus of A<sub>1</sub>AR, A<sub>2A</sub>AR or A<sub>2B</sub>AR was fused to SmBiT, while LgBiT was fused to the N-  
515 terminus of G proteins. The C terminus of A<sub>3</sub>AR was fused with LgBiT, and the SmBiT element  
516 was fused to the N terminus of G proteins. HEK293 cells were seeded at  $4 \times 10^4$  cells/well on  
517 96-well plates and co-transfected with AR-SmBit and LgBiT-G protein plasmids at a 1:1 mass  
518 ratio. After 24 hours, cells were replaced with 40 µL fresh culture medium without fetal bovine  
519 serum. Ten microliter Nano-Glo Live Cell reagent was added followed the manufacturer's  
520 protocol (Promega, N2011), and incubated at 37 °C, 5 % CO<sub>2</sub> for 5 min. Another 25 µL culture  
521 medium containing various concentrations of compounds were added and incubated at room  
522 temperature for 10 minutes before measuring bioluminescence using EnVision multiplate  
523 reader (PerkinElmer).  
524

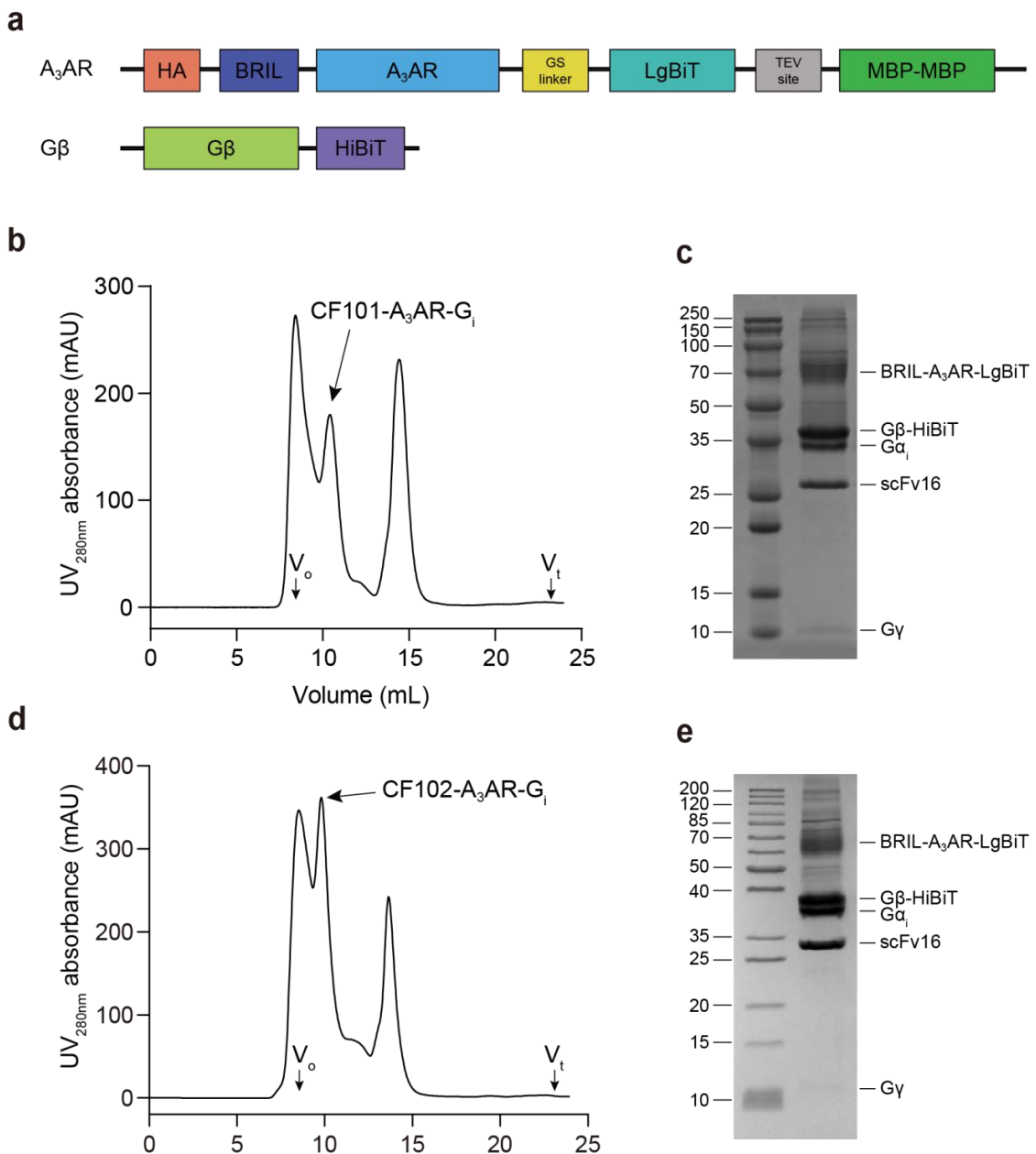
525  
526  
527  
528  
529  
530  
531  
532  
533  
534  
535  
536  
537

### Cell-surface expression assay

Wild type A<sub>1</sub>AR, A<sub>2A</sub>AR, A<sub>2B</sub>AR or A<sub>3</sub>AR gene was subcloned into pcDNA3.0 vector with an N-terminal human influenza hemagglutinin tag (HA-tag). HEK293 were seeded at 4 × 10<sup>4</sup> cells/well on 96-well plates and transfected with wild type (WT) or adenosine receptor mutants. After 24 hours, cells were washed with PBS buffer, fixed with 4 % (w/v) paraformaldehyde for 15 min, and blocked with 2 % (w/v) bovin serum albumin (BSA) for 1 h. Next, cells were incubated with the polyclonal anti-HA (Sigma, H6908) overnight at 4 °C, followed by 1 h with horseradish peroxidase (HRP)-conjugated anti-rabbit antibody (Cell Signaling, 7074S) at room temperature. After washing, 50 µL tetramethylbenzidine (Sigma, T0440) was added for 30 min before stopping the reaction with 25 µL TMB substrate stop solution (Beyotime, P0215). Absorbance at 450 nm was measured on a FlexStation III microplate reader (Molecular Devices).

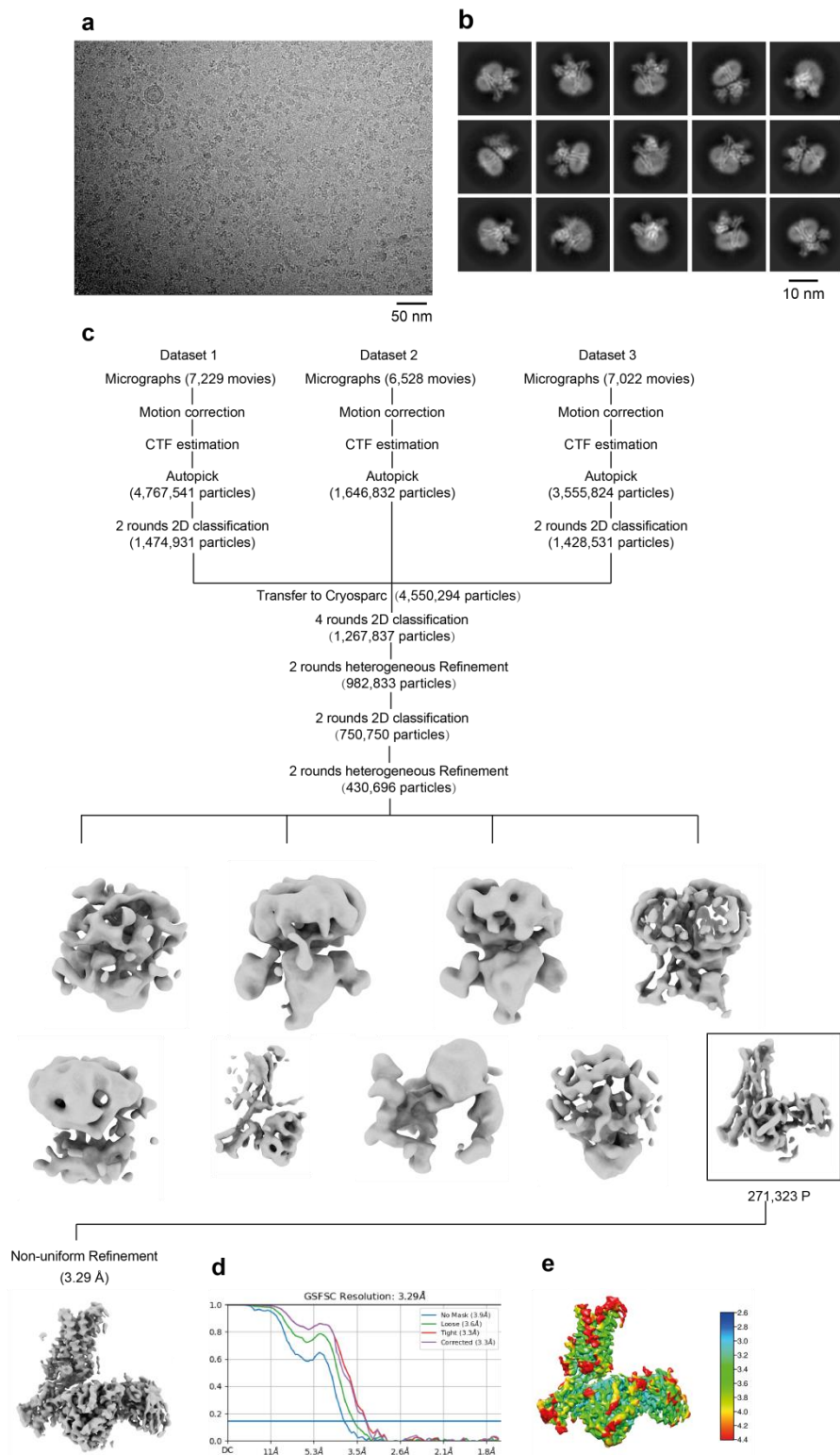
### Statistical analysis

All functional study data were analyzed in Prism 8 (GraphPad) and presented as means ± S.E.M. from at least three independent experiments. Concentration-response curves were evaluated with a three-parameter logistic equation. EC<sub>50</sub> values were calculated using the sigmoid three-parameter equation. Significance was determined by one-way ANOVA followed by multiple comparisons test, and \*P < 0.05 vs. wild-type (WT) was considered statistically significant.



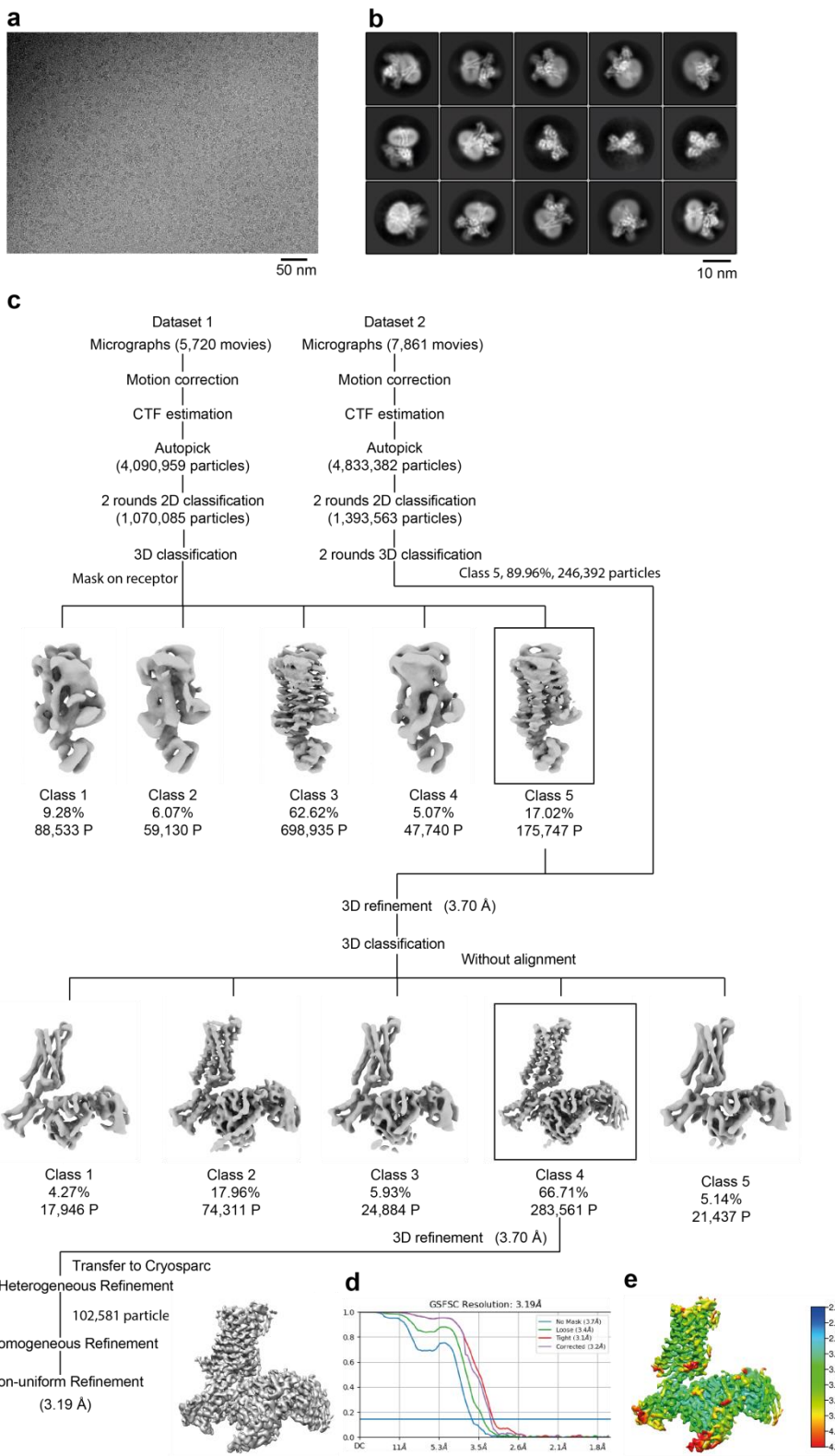
**Supplementary Fig. 1 The expression and purification of A<sub>3</sub>AR-G<sub>i</sub> complex.**

**a.** Schematic diagrams of the expression constructs of A<sub>3</sub>AR and G<sub>β</sub>1 using the NanoBiT tethering approach. A<sub>3</sub>AR and G<sub>β</sub>1 fused with LgBiT and HiBiT, respectively. **b.** Size-exclusion chromatography profile of the CF101-A<sub>3</sub>AR-G<sub>i</sub> complex. **c.** SDS-PAGE of the arrow indicated peak fraction in (b). **d.** Size-exclusion chromatography profile of the CF102-A<sub>3</sub>AR-G<sub>i</sub> complex. **e.** SDS-PAGE of the arrow indicated peak fraction in (d).



553  
554 **Supplementary Fig. 2 Cryo-EM data processing of CF101-A<sub>3</sub>AR-G<sub>i</sub> complex.**

555 **a.** Representative image from cryo-EM dataset. Scale bar, 50 nm. **b.** Respresentative 2D  
556 average classification classes. Scale bar, 10 nm. **c.** Flow-chart of the cryo-EM data  
557 processing. **d.** FSC curves. **e.** The local resolution map.

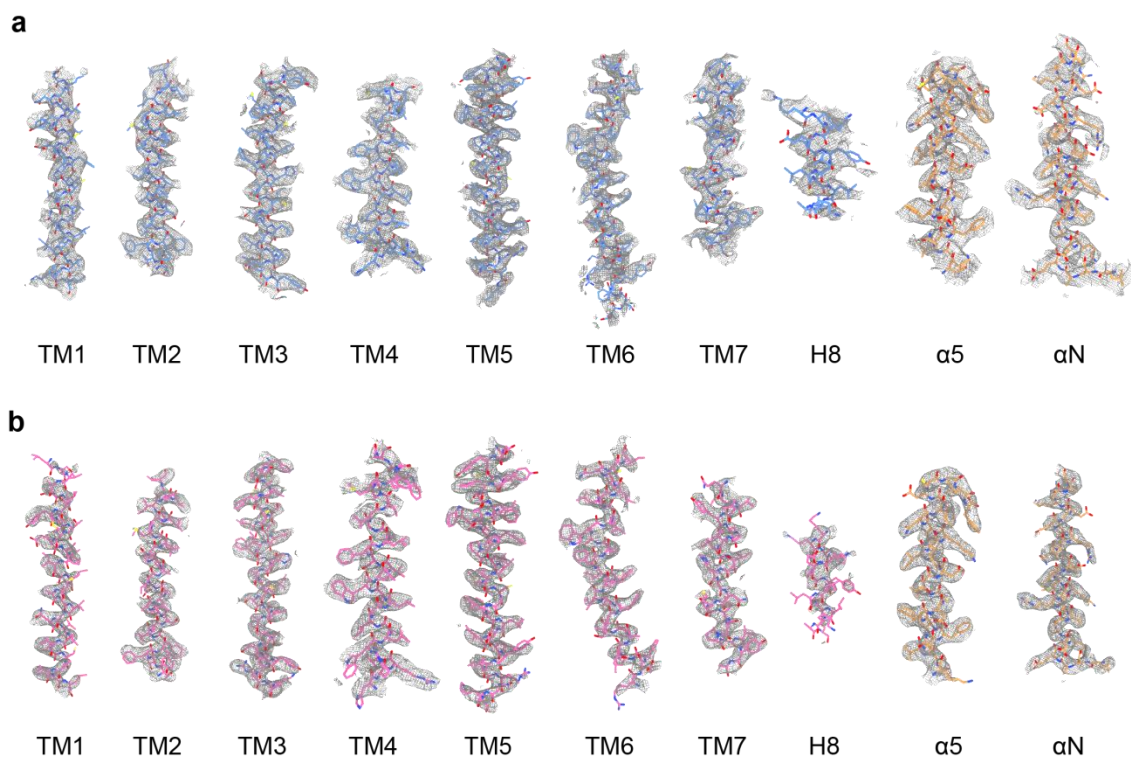


**Supplementary Fig. 3 Cryo-EM data processing of CF102-A<sub>3</sub>AR-G<sub>i</sub> complex.**

558  
 559 **a.** Representative image from cryo-EM dataset. Scale bar, 50 nm. **b.** Respresentative 2D  
 560 average classification classes. Scale bar, 10 nm. **c.** Flow-chart of the cryo-EM data  
 561 processing. **d.** FSC curves. **e.** The local resolution map.  
 562

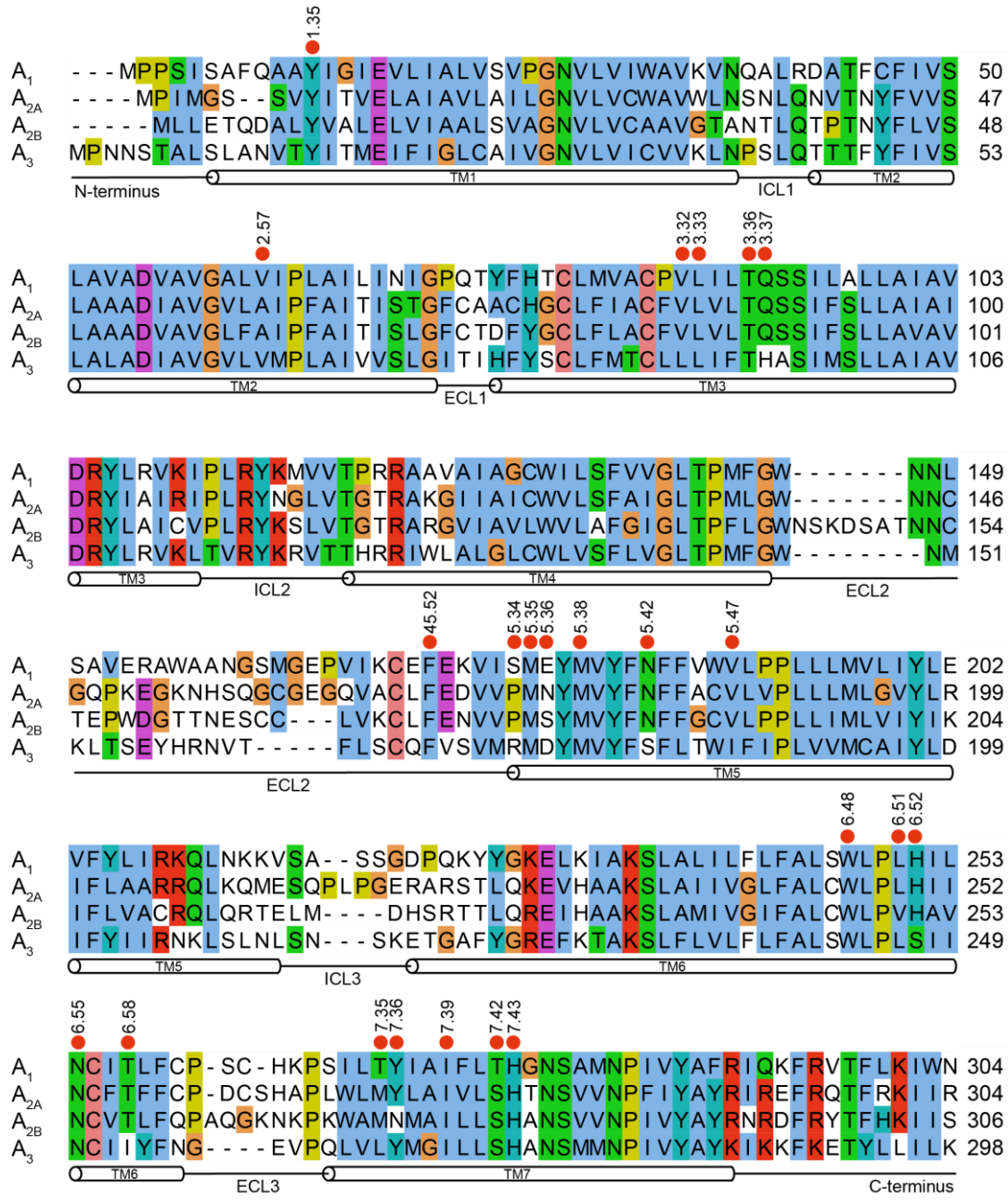
563

564

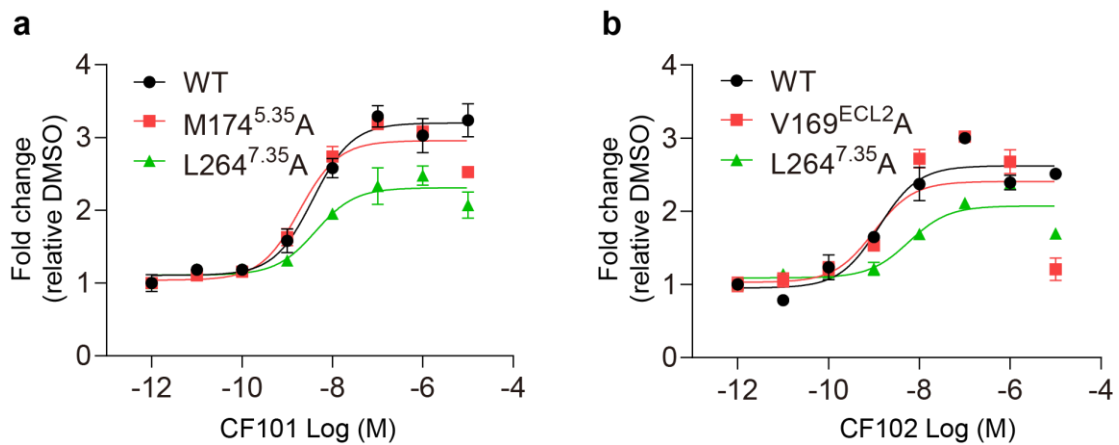


565  
566  
567  
568  
ChinaXiv:2023.1/00051v1

**Supplementary Fig. 4** Representative regions of cryo-EM density maps are shown for the each transmembrane helical (TM) of A<sub>3</sub>AR and the  $\alpha$ 5 and  $\alpha$ N helices of G $\alpha$ i.

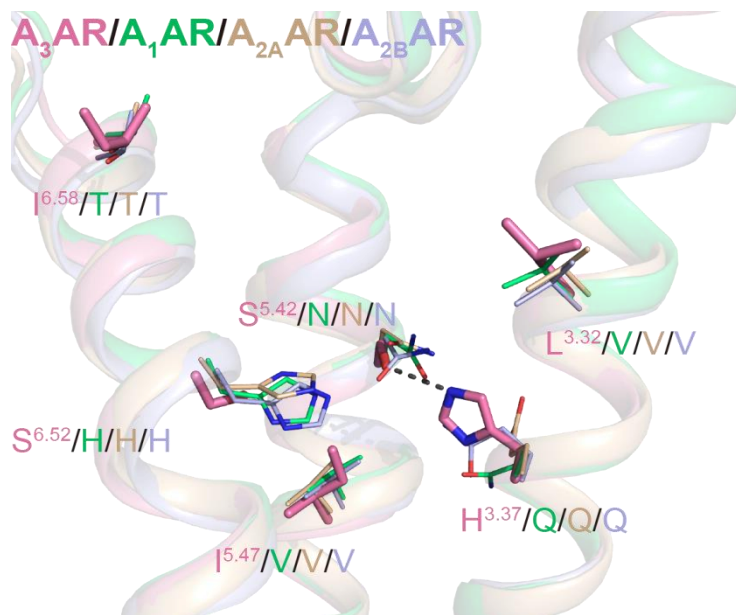


570 **Supplementary Fig. 5 Sequence alignment of adenosine receptors.** The sequence  
 571 alignment was generated with Jalview<sup>[42]</sup> and depicts the N-/C-terminus, transmembrane  
 572 helices (TMs), extracellular loops (ECLs), and intracellular loops (ICLs). Residues lining the  
 573 orthosteric binding site are highlighted with red circles and annotated with GPCR  
 574 Ballesteros-Weinstein numbering scheme. The C-terminus of the adenosine receptors were  
 575 omitted.  
 576



577  
578 **Supplementary Fig. 6 Effects of CF101 or CF102 on the A<sub>3</sub>AR mutants.** These residues  
579 in A<sub>3</sub>AR formed hydrophobic interactions with the 3-iodophenyl group present in CF101 and  
580 CF102.  
581  
582  
583

584

**Supplementary Fig. 7 The orthosteric binding pockets among adenosine receptors.**

The positions highlighted indicate where unique residues occurred in A<sub>3</sub>AR compared to other adenosine receptors. The receptor names and their associated colors are shown above the models. The side chains in A<sub>3</sub>AR were depicted as bold sticks, while the corresponding side chains in other adenosine receptors were shown as thick sticks.

591

592

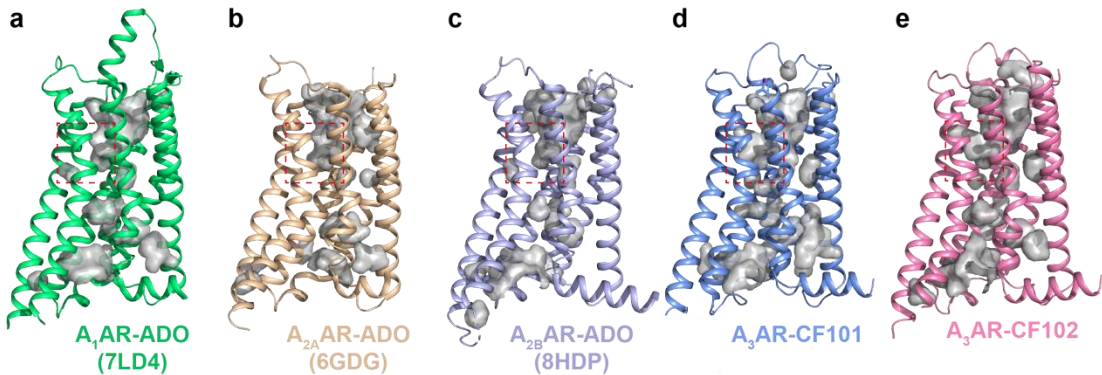
593

594

595

596

Chinaxiv:202311.00051v1



**Supplementary Fig. 8 The binding cavities in adenosine receptors.**

**a-e** The binding cavities of the adenosine receptors are depicted as gray surfaces, with the bound ligands shown as sticks. The receptor names and associated PDB codes<sup>[21, 24, 43]</sup> are indicated below each model. The unique subpocket in the A<sub>3</sub>AR as the red boxes circled.

**Supplementary Table 1 Cryo-EM data collection, model refinement and validation statistics.**

	A <sub>3</sub> AR-CF101-G <sub>i</sub> complex	A <sub>3</sub> AR-CF102-G <sub>i</sub> complex
<b>Data collection and processing</b>		
Detector	K3	K3
Magnification	105,000	105,000
Voltage (kV)	300	300
Electron exposure (e <sup>-</sup> /Å <sup>2</sup> )	50	50
Defocus range (μm)	-1.0~-3.0	-1.0~-3.0
Pixel size (Å)	0.824	0.824
Symmetry imposed	C1	C1
Initial particle projections (no.)	9,970,197	8,924,341
Final particle projections (no.)	271,323	102,581
Map resolution (Å)	3.29	3.19
Map resolution range (Å)	2.60-4.40	2.40-4.20
FSC threshold	0.143	0.143
<b>Model Refinement</b>		
Refinement package	PHENIX-1.17.1-3660	PHENIX-1.17.1-3660
Real or reciprocal space	Real space	Real space
Model-Map CC (mask)	0.60	0.72
Model resolution (Å)	4.10	3.40
FSC threshold	0.5	0.5
B factors (Å <sup>2</sup> , min/max/mean value)		
Protein residues	30.00/127.38/68.24	30.00/135.93/68.27
Ligands	20.00/20.00/20.00	20.00/20.00/20.00
<b>Model composition</b>		
Non-hydrogen atoms	8,751	8,753
Protein residues	1,126	1,127
R.m.s. deviations		
Bond lengths (Å)	0.001	0.005
Bond angles (°)	0.398	0.900
<b>Validation</b>		
MolProbity score	1.46	1.15
Clashscore	8.51	3.62
Rotamer outliers (%)	0.00	0.00
Ramachandran plot		
Favored (%)	98.19	98.38
Allowed (%)	1.81	1.62
Disallowed (%)	0.00	0.00
<b>Data availability</b>		
EMDB code		
PDB code		

600  
601 **Supplementary Table 2 Cell surface expression of A<sub>3</sub>AR and its mutants on CF101- and**  
602 **CF102-induced NanoBiT assay.**

	EC <sub>50</sub> (nM) <sup>a</sup>		Cell-surface expression (Relative to WT) <sup>a</sup>
	CF101	CF102	
WT	3.74±0.7	1.50±0.4	100±2.5
Y15 <sup>1.35</sup> A	UD <sup>b</sup>	UD	113±5.0
L90 <sup>3.32</sup> V	2.71±0.6	3.94±0.5	79.6±6.8
L91 <sup>3.33</sup> A	UD	UD	107±12.1
T94 <sup>3.36</sup> A	UD	UD	91.5±4.7
H95 <sup>3.37</sup> A	UD	UD	121±7.1
H95 <sup>3.37</sup> Q	7.70±3.9	5.01±1.6	124±5.6*
F168 <sup>ECL2</sup> A	>10000	UD	116±4.0
V169 <sup>ECL2</sup> A	NT <sup>c</sup>	1.07±0.3	85.9±6.0
M174 <sup>5.35</sup> A	1.973±0.5	NT	85.0±2.3
M177 <sup>5.38</sup> A	>10000	UD	110±1.4
S181 <sup>5.42</sup> A	UD	UD	102±5.3
S181 <sup>5.42</sup> N	UD	UD	88.8±4.1
I186 <sup>5.47</sup> A	UD	UD	79.2±2.7
I186 <sup>5.47</sup> V	10.64±2.3	29.96±7.1***	93.6±2.3
W243 <sup>6.48</sup> A	>10000	UD	65.5±6.2**
L246 <sup>6.51</sup> A	>10000	UD	81.0±4.9
S247 <sup>6.52</sup> H	>10000	UD	82.5±6.2
N250 <sup>6.55</sup> A	UD	UD	78.2±5.0
I253 <sup>6.58</sup> T	17.04±4.1**	13.11±4.5	90.1±9.8
L264 <sup>7.35</sup> A	4.08±0.8	5.53±1.5	73.7±3.8*
I268 <sup>7.39</sup> A	UD	UD	67.4±4.2**
H272 <sup>7.43</sup> A	UD	UD	12.7±3.6***

603  
604 <sup>a</sup>Data shown are means ± S.E.M. from at least three independent experiments.

605 <sup>b</sup>UD indicates that the activation level is too low to determine EC<sub>50</sub> values.

606 <sup>c</sup>NT, not test.

607 \* P<0.01; \*\*P<0.001 and \*\*\*P<0.0001 by one-way ANOVA followed by multiple comparisons  
608 test, compared with WT.

612  
613 **Supplementary Table 3 Cell surface expression of A<sub>1</sub>AR/A<sub>2A</sub>AR/A<sub>2B</sub>AR and its relative  
mutant on CF101- and CF102-induced NanoBiT assay.**

Receptor	CF101		CF102		Cell-surface expression (Relative to WT) <sup>a</sup>
	EC <sub>50</sub> (nM) <sup>a</sup>	max change (Relative to basal) <sup>a</sup>	EC <sub>50</sub> (nM)	max change (Relative to basal)	
A <sub>1</sub> AR	206.8±55	1.19±0.1	>10000	2.12±0.1	100±1.5
A <sub>1</sub> AR-ECL3	161.9±36	3.69±0.2***	176.6±102	3.86±0.6**	91.1±3.2
A <sub>2A</sub> AR	1280±727	1.53±0.1	UD <sup>b</sup>	1.03±0.1	100±2.9
A <sub>2A</sub> AR-ECL3	74.29±16	2.21±0.1*	48.04±28	1.84±0.1	92.1±1.6
A <sub>2B</sub> AR	>10000	1.77±0.1	UD	0.95±0.1	100±7.6
A <sub>2B</sub> AR-ECL3	1952±289	4.06±0.2***	>10000	2.72±0.2**	80.5±1.9**

614  
615 <sup>a</sup>Data shown are means ± S.E.M. from at least three independent experiments.

616 <sup>b</sup>UD indicates that the activation level is too low to determine EC<sub>50</sub> values.

617 \* P<0.01; \*\*P<0.001 and \*\*\*P<0.0001 by one-way ANOVA followed by multiple comparisons  
618 test, compared with WT.  
619

## References

20. Duan, J, DD Shen, XE Zhou, P Bi, QF Liu, YX Tan, YW Zhuang, HB Zhang, et al., Cryo-EM structure of an activated VIP1 receptor-G protein complex revealed by a NanoBiT tethering strategy. *Nat Commun*, 2020. 11(1): 4121.
21. Cai, H, Y Xu, S Guo, X He, J Sun, X Li, C Li, W Yin, et al., Structures of adenosine receptor A(2B)R bound to endogenous and synthetic agonists. *Cell Discov*, 2022. 8(1): 140.
24. Draper-Joyce, CJ, R Bhola, J Wang, A Bhattacharai, ATN Nguyen, I Cowie-Kent, K O'Sullivan, LY Chia, et al., Positive allosteric mechanisms of adenosine A(1) receptor-mediated analgesia. *Nature*, 2021. 597(7877): 571-576.
29. Liu, P, MZ Jia, XE Zhou, PW De Waal, BM Dickson, B Liu, L Hou, YT Yin, et al., The structural basis of the dominant negative phenotype of the Galphai1beta1gamma2 G203A/A326S heterotrimer. *Acta Pharmacol Sin*, 2016. 37(9): 1259-72.
30. Maeda, S, A Koehl, H Matile, H Hu, D Hilger, GFX Schertler, A Manglik, G Skiniotis, et al., Development of an antibody fragment that stabilizes GPCR/G-protein complexes. *Nat Commun*, 2018. 9(1): 3712.
31. Rohou, A and N Grigorieff, CTFFIND4: Fast and accurate defocus estimation from electron micrographs. *J Struct Biol*, 2015. 192(2): 216-21.
32. Zheng, SQ, E Palovcak, JP Armache, KA Verba, Y Cheng and DA Agard, MotionCor2: anisotropic correction of beam-induced motion for improved cryo-electron microscopy. *Nat Methods*, 2017. 14(4): 331-332.
33. Zivanov, J, T Nakane, BO Forsberg, D Kimanius, WJ Hagen, E Lindahl and SH Scheres, New tools for automated high-resolution cryo-EM structure determination in RELION-3. *Elife*, 2018. 7.
34. Punjani, A, JL Rubinstein, DJ Fleet and MA Brubaker, cryoSPARC: algorithms for rapid unsupervised cryo-EM structure determination. *Nat Methods*, 2017. 14(3): 290-296.
35. Jumper, J, R Evans, A Pritzel, T Green, M Figurnov, O Ronneberger, K Tunyasuvunakool, R Bates, et al., Highly accurate protein structure prediction with AlphaFold. *Nature*, 2021. 596(7873): 583-589.
36. Liu, Q, D Yang, Y Zhuang, TI Croll, X Cai, A Dai, X He, J Duan, et al., Ligand recognition and G-protein coupling selectivity of cholecystokinin A receptor. *Nat Chem Biol*, 2021. 17(12): 1238-1244.
37. Pettersen, EF, TD Goddard, CC Huang, GS Couch, DM Greenblatt, EC Meng and TE Ferrin, UCSF Chimera--a visualization system for exploratory research and analysis. *J Comput Chem*, 2004. 25(13): 1605-12.
38. Emsley, P and K Cowtan, Coot: model-building tools for molecular graphics. *Acta Crystallogr D Biol Crystallogr*, 2004. 60(Pt 12 Pt 1): 2126-32.
39. Adams, PD, K Gopal, RW Grosse-Kunstleve, LW Hung, TR Ioerger, AJ McCoy, NW Moriarty, RK Pai, et al., Recent developments in the PHENIX software for automated crystallographic structure determination. *J Synchrotron Radiat*, 2004. 11(Pt 1): 53-5.
40. Croll, TI, ISOLDE: a physically realistic environment for model building into low-resolution electron-density maps. *Acta Crystallogr D Struct Biol*, 2018. 74(Pt 6): 519-530.
41. Pettersen, EF, TD Goddard, CC Huang, EC Meng, GS Couch, TI Croll, JH Morris and TE Ferrin, UCSF ChimeraX: Structure visualization for researchers, educators, and developers. *Protein Sci*, 2021. 30(1): 70-82.

- 664  
665  
666  
667  
668
42. Waterhouse, AM, JB Procter, DM Martin, M Clamp and GJ Barton, Jalview Version 2--a multiple sequence alignment editor and analysis workbench. *Bioinformatics*, 2009. 25(9): 1189-91.
  43. Garcia-Nafria, J, Y Lee, X Bai, B Carpenter and CG Tate, Cryo-EM structure of the adenosine A(2A) receptor coupled to an engineered heterotrimeric G protein. *Elife*, 2018. 7.